**Wind and Structures**, *Vol. 22, No. 2 (2016) 133-160*
DOI: http://dx.doi.org/10.12989/was.2016.22.2.133


# Towards guidelines for design of loose-laid roof pavers for wind uplift

Maryam Asghari Mooneghi[1a], Peter Irwin[2b] and Arindam Gan Chowdhury[*2]

[1]*Advanced Technology and Research, Arup, San Francisco, CA, USA*
[2]*Department of Civil and Environmental Engineering/International Hurricane Research Center, Florida International University, Miami, FL, USA*

*(Received June 3, 2014, Revised October 28, 2015, Accepted November 2, 2015)*

**Abstract.** Hurricanes are among the most costly natural hazards to impact buildings in coastal regions. Building roofs are designed using the wind load provisions of building codes and standards and, in the case of large buildings, wind tunnel tests. Wind permeable roof claddings like roof pavers are not well dealt with in many existing building codes and standards. The objective of this paper is to develop simple guidance in code format for design of loose-laid roof pavers. Large-scale experiments were performed to investigate the wind loading on concrete roof pavers on the flat roof of a low-rise building in Wall of Wind, a large-scale hurricane testing facility at Florida International University. They included wind blow-off tests and pressure measurements on the top and bottom surfaces of pavers. Based on the experimental results simplified guidelines are developed for design of loose-laid roof pavers against wind uplift. The guidelines are formatted so that use can be made of the existing information in codes and standards such as American Society of Civil Engineering (ASCE) 7-10 standard's pressure coefficients for components and cladding. The effects of the pavers' edge-gap to spacer height ratio and parapet height to building height ratio are included in the guidelines as adjustment factors.

**Keywords:** design guidelines; roof pavers; large-scale testing; wind uplift

## 1. Introduction

It is clearly important that roofing materials be designed so that they can withstand the uplift forces that occur in strong winds. Some of the major losses that have occurred in hurricanes have been due to loss of roofing materials (Huang e*t al*. 2009). Experience indicates that hurricane winds are well capable of ripping off materials such as tiles, shingles, roof pavers and gravel ballast (Smith 1994, Huang *et al*. 2009). The building itself then becomes vulnerable to considerable additional damage through water infiltration and changes in internal pressure (Bitsuamlak *et al.* 2009, Chowdhury *et al*. 2012). As well, the wind-borne debris coming from the damaged roof often causes extensive additional damage to buildings downwind as it impacts them with high momentum (Fernandez *et al.* 2010, Masters *et al*. 2010).

∗Corresponding author, Associate Professor, E-mail: chowdhur@fiu.edu
[a] Ph.D., E-mail: maryam.asghari@arup.com
[b] Professor of Practice, E-mail: peairwi@fiu.edu

**Copyright © 2016 Techno-Press, Ltd.**
http://www.techno-press.org/?journal=was&subpage=8 ISSN: 1226-6116 (Print), 1598-6225 (Online)

Wind uplift of roof pavers is not only the result of the suction on their top surface, but also of the pressure on their underside for which no guidance is currently supplied in most wind codes. Therefore, for lack of better information, building designers often make the simplifying assumption that the net uplift acting on air permeable roofing elements is the same as the exterior pressure specified in the building code (Florida Public Hurricane Loss Projection Model (FPHLPM) 2005). In reality a significant amount of pressure equalization occurs which tends to make this assumption quite conservative in many instances for roof pavers (Banks *et al*. 2000). On the other hand, the pressure equalization effect is subject to a number of influencing variables such as paver's location relative to a corner, paver size and geometry, parapet height, building height, gaps between pavers, and the stand-off distance of the pavers above the underlying roof surface (Bienkiewicz and Sun 1997, Banks *et al.* 2000). This has deterred the development of more specific guidance in codes. Interlocking and strapping systems are often used to improve the resistance of roof pavers, and they can be very effective (Irwin *et al.* 2012). However failures do still occur and it will help in the design of such systems if better knowledge of the aerodynamic forces working on the pavers can be obtained. The aerodynamic mechanisms that cause uplift are quite complex but in this paper guidance is developed in the form of relatively simple rules for the design of loose-laid roof pavers against uplift wind forces, rules that are amenable to use alongside or within building codes.

A set of large-scale experiments was performed to study the wind loading mechanism of concrete roof pavers using the Wall of Wind (WOW) facility at Florida International University (FIU). Concrete pavers were installed on a square portion of a flat roof of a low-rise building. Both wind blow-off testing and pressure measurements were performed. Experiments included the wind lift-off tests and detailed pressure measurements on the external and underneath surfaces of roof pavers. The effects of the pavers' edge gap to spacer height ratio, relative parapet height and the effects of connecting pavers were studied. The results from the pressure measurements were compared with estimates obtained from American Society of Civil Engineering (ASCE) 7-10 pressure coefficients. Finally, guidelines were proposed for design of loose-laid roof pavers using ACSE 7-10 components and cladding exterior pressure coefficients taking into account the effects of pavers' edge-gap to spacer height ratio, relative parapet height, and pressure equalization.

## 2. Background

Solid pavers are frequently used as ballast and walking surfaces on flat roofs and as decorative elements on terraces. It is necessary that they be capable of resisting uplift forces due to wind. A number of experimental and analytical studies are reported on wind loading and performance of loose-laid roofing systems. Wind tunnel experiments on small scale models have been performed by researchers to investigate the wind loading and failure mechanism of loose-laid roof paving system (Kind and Wardlaw 1979, Kind and Wardlaw 1982, Bienkiewicz and Sun 1992, Bienkiewicz and Sun 1997, Irwin *et al.* 2012, Oh and Kopp 2015). Large-scale testing is preferred for small structures and building appurtenances for maintaining modeling accuracy and minimizing Reynolds number effects (Kargarmoakhar *et al*. 2015). However, studies using full- and large-scale models (Aly *et al*. 2012, Asghari Mooneghi *et al.* 2014) have been limited. As explained by Geurts (2000), small scale wind tunnel experiments are not normally suitable for investigating the pressure equalization over air permeable roof covering materials and its effects on the net loading. This is because when the batten space and permeability are scaled, their sizes get too small to simulate the realistic mechanisms in the flow due to Reynolds number effects. Therefore, large scale test data or full scale field measurements are necessary for proposing calculation models and design guidelines for these materials.

The complex nature of the flows above and beneath air permeable roofing systems has also been explored using numerical simulations. Amano *et al*. (1988) proposed a simplified numerical model based on the unsteady Bernoulli equation with one value of pressure at each paver edge for obtaining the internal wind pressure distribution of roof pavers under a known external pressure field. Correction terms were employed to take into account the effects of viscosity. The effect of the gap between the pavers was also investigated. Kind *et al*. (1988) proposed a correlation for predicting wind lift-off speeds of loose-laid insulation boards based on extensive wind tunnel testing results. The correlation accounts for the effects of building characteristics (low, intermediate or high–rise building), parapet height, element weight per unit area and interlock effects. The tests of Kind *et al*. (1988) were primarily for pavers laid directly on the roof with no spacers underneath. Gerhardt *et al.* (1990) performed a set of experiments and calculations and developed an equation for calculating the failure wind speed based on the external pressure, the element size relative to smaller plan dimension of the building and the weight of the elements. Diagrams were provided to help choose the best possible solution when using these roofing systems. Sun and Bienkiewicz (1993) stated that the flows between and beneath the loose-laid pavers are very slow because of the boundary effects of the flow field, and should be treated as viscous. They employed Darcy's law to develop a numerical model for calculating the pressure distribution underneath roof pavers. In their model, the pressure distribution along paver edges was assumed piecewise linear. The experimental data and their numerical results show similar trends. This model was refined later to allow arbitrary pressure distribution along paver edges, and to take into account the interlock effects between pavers. This flow model was limited to steady flow and was sufficient to estimate the mean pressure distribution for small stand-off distances between the roof surface and pavers and for low speeds of the flow, which means low Reynolds number. However, it may not be so applicable for a relatively high flow speed with high turbulence (Oh and Kopp 2012). Kind (1994) proposed a numerical method based on Laplace’s equation for predicting the underneath pressure distribution for loose laid roof pavers. It was assumed that inertia effects are negligible in the under-element flow and it was thought to be viscosity dominated. Also, the flow resistance in the element/roof deck interface plane was considered as uniform. With these assumptions the flow continuity equation reduces to the Laplace equation. The results were in reasonable agreement with measured pressure distributions in cases where the roof deck and the undersides of the elements were reasonably flat with uniform surface texture. The results are more likely to be applicable for pavers lying directly on the roof surface. Bofah et al. (1996) proposed a theory for calculating the pressure distribution underneath roof pavers based on approximating the underneath flow by a two-dimensional laminar flow in a very shallow channel with a porous upper roof. Sinusoidal and uniform outer pressure distributions were investigated which were consistent with experimental results. Trung *et al*. (2010) applied a method based on the Multiple Discharge Equations (MDE) as described in Oh *et al.* (2007) to predict the underneath pressures of a porous sunshade roof cover from a known external pressure distribution. Computational results were compared with experiments performed on a 1:50 scale model of a low-rise building. The results of the computations were in good agreement with the experiments for 5% and 10% porosity ratios (ratio between the areas of orifices to the area of the sheet) and 4.7 mm height from the roof deck to the cover used in the experiments. Oh and Kopp (2014) developed a one-dimensional analytical model for simulating cavity pressures within multi-layer roofing systems from a known external pressure distribution using the unsteady Bernoulli equation and Couette flow assuming laminar flow in the cavity. The model was verified by comparing its predictions with results obtained from wind tunnel testing.

Previous experimental and numerical studies on the wind loading mechanism of loose-laid roofing systems like roof pavers, gravel ballast, green roofs, etc. can assist in developing code specific models for design of such systems. However, many unanswered questions still remain in the current state of knowledge on this issue. In research aimed at codification of wind loading on porous claddings and covers over roofs which have a similar wind loading mechanism as roof pavers, Cheung and Melbourne (1986) and Cheung and Melbourne (1988) investigated the effect of porosity on wind loading on such systems. Reduction factors were proposed as a function of distance from the roof leading edge for different porosities and different internal volumes for a typical low-pitch roof cladding, and adopted by AS/NZS 1170.2. Design wind loads could then be estimated from external pressure coefficients given in the existing building codes. Bienkiewicz and Meroney (1988) developed a rough design guideline for loose-laid ballast pavers. The system failure condition was considered in terms of the failure wind speed and the wind loading parameters specified by the building code parameters (UBC, ANSI or ASCE 7-05 (Bienkiewicz and Endo 2009). This theory is limited to low buildings with rectangular flat roofs. The allowable building heights are given in the design guidelines for a range of design wind speeds and wind exposures.

Some codes and standards do address the design of roof paver systems. In the Netherlands code, NEN EN 1991-1-4/NA, a set of values for net pressure coefficients (difference between the external and underneath pressure coefficients; $Cp_{net}=Cp_e-Cp_i$) is proposed for design of roofing tiles and pavers. These values were based on a number of experiments and full-scale studies on roof tiles on pitched roofs and roof pavers on flat roofs including those of Geurts (2000), who proposed equalization factors defined as $C_{eq}=Cp_{net}/Cp_e$ from full-scale measurements on roof tiles and roof pavers. The equalization factors are to be applied to the external pressure coefficients given in the Netherlands wind loading code. The proposed value of $C_{eq}$ for roof pavers with and without interlock were 0.25 and 0.6, respectively. In the German Wind Code (DEUTSCHE NORM 2001-03) design pressure coefficients are provided for building envelopes with permeable facades based on a study by Gerhardt and Janser (1995). In the Australian Standard for wind loads (AS 1170.2 2011) reduction factors are given for estimating design wind loads on porous claddings. These factors depend on the cladding porosity and the horizontal distance from windward building edge, and are based on the work of Cheung and Melbourne (1988).

Major international codes and standards for wind loads in USA and Canada (NBCC; ASCE 7-10) specify roof wind pressures for typical roof geometries but there are no specific provisions on how to apply such pressures to roofing elements such as tiles, shingles, and pavers. Using the available numerical methods proposed in literature for designers and suppliers of roof pavers is quite complex, and performing project specific wind tunnel testing is not practical, except for very large projects. This paper proposes a simplified yet reasonably accurate method for calculating the net uplift force on roof paver systems from the existing external pressure coefficients in the current ASCE 7-10 standard and takes into account the effect of pavers' edge gap to spacer height ratio, relative parapet height, and pressure equalization.

## 3. Pressure gradient effects

Multi-layer building envelopes, e.g. roof pavers are particularly sensitive not just to pressures but to spatial pressure gradients. Concrete roof pavers are usually placed on the roof with spacing above the roof deck and with gaps between the pavers. The pressure distribution produced by the wind flow over the outer surface of the roof produces secondary flows through the spaces between and underneath the paver elements. The so called pressure equalization occurs very quickly, provided the space between the pavers and the roof deck below is not too large, typically in a small fraction of a second, because very small volumes of air exchange are needed to bring the underside pressure into equilibrium with the pressures around the paver perimeter. This phenomenon is controlled by the same physics as the internal pressure. However, in pressure equalization, much smaller volumes of air through many openings are involved. The pressure equalization effect greatly reduces the net uplift force on pavers in most areas of a roof. However, in areas of very high spatial gradients of pressure, such as those which occur under vortices near roof corners, significant net uplift pressures can still occur. Figure 1 illustrates the typical path of the vortices over a flat roof for cornering winds.

Along with the high suctions from the vortices there are also high velocities passing over the surface as the flow rotates rapidly about the vortex center. The vortex is analogous to a small tornado with axis approximately horizontal and with very high velocities near the vortex core. Thus, not only are there high suctions tending to lift roofing material, but also high tangential air speeds immediately adjacent to the roof surface, which are prone to penetrating under the edges of roofing elements and lifting them. It is very important to generate these vortices as part of the test to fully replicate these wind effects on a roof. The bell-shaped curves in Fig. 1 have greatest central suction near the roof corner but as distance from the roof corner increases, the suction reduces and the width of the bell-shape grows larger (Banks *et al.* 2000). The effect of these suction distributions on the roof will depend on the type of roof system being used and is clearly very different from a simple uniform pressure distribution. The diagram in Fig. 2 illustrates schematically the general mechanism of uplift on roof pavers. The aerodynamic uplift force is the difference between the pressure on the lower surface of the paver, $P_L$ and the pressure on the upper surface, $P_U$ (Fig. 2). The pressure on the upper surface due to the presence of a conical vortex (solid curve) is negative (when measured relative to the static pressure in the surrounding air stream) and has a concentrated peak.

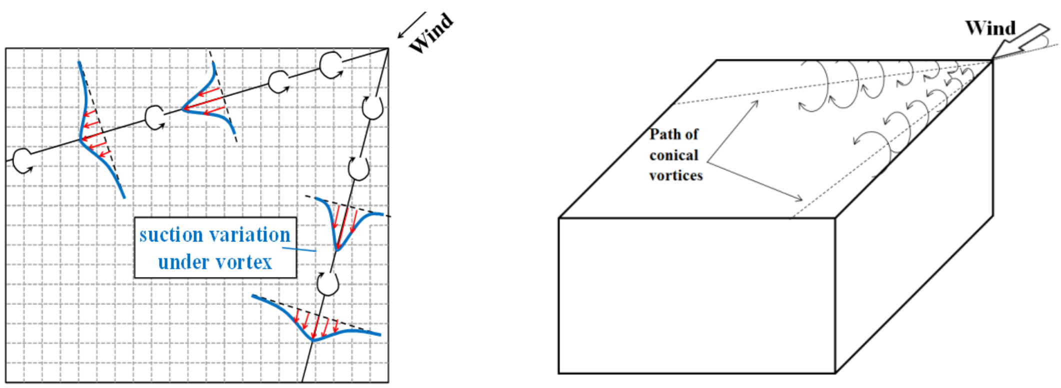


Fig. 1 Conical vortices; Suction variation on roof under corner vortices

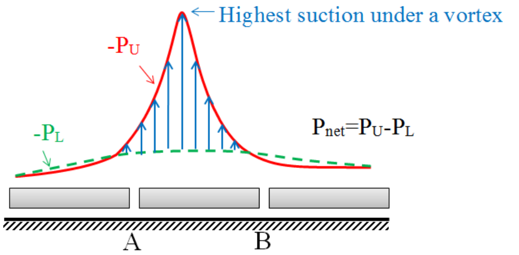


(a) Pressure distributions on upper and lower surfaces of a roof paver

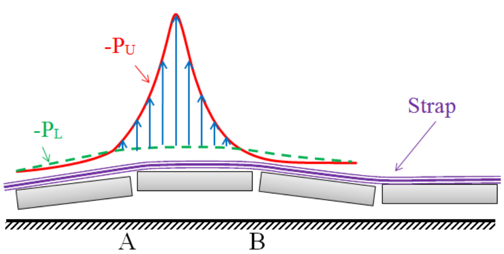


(b) Straps running transverse to the axis of the vortex

Fig. 2 General mechanism of uplift on roof pavers

The pressure on the lower surface is depicted by the broken curve and at the paver edge it is shown as being equal to that on the top surface. In practice, the top and bottom edge pressures do not always match exactly. The underneath pressure is dictated by the outer pressure distribution and the relative magnitude of the joint resistances compared to the under-element resistance which prevents a complete pressure equilibration between upper and lower surfaces of the element (Bofah *et al*. 1996, Gerhardt *et al.* 1990, Kind 1994). Detailed measurements done by Kind and Wardlaw (1982) showed that the underneath pressure does tend to vary roughly linearly between the pressures at the paver edges as depicted in Fig. 2 (also discussed in Bofah *et al.* (1996)). It is only due to the sharp peak of the upper pressure under a vortex (between points A and B) that a net uplift might occur, signified by the large difference between the solid and broken curves. If the upper surface pressure does not have the peak (e.g., the pavers are not sitting directly under a vortex) then pressure equalization caused by flow around the edges of the paver results in much smaller net uplift as shown by the small differences between the solid and dashed curves on the pavers outside of the zone between points A and B. The impact of pressure equalization depends on the size of the paver relative to the width of the conical vortex. If the paver is much larger than the width of the vortex then the impact is reduced since only a small fraction of the paver area is affected by the high suction. Also, if the paver is much smaller than the width of the vortex then, even if it is sitting in a high suction zone, the pressure equalization effect of the gaps at its edges substantially reduces the difference in pressure between top and bottom surfaces. If the paver and vortex widths are similar the net uplift will tend to be maximized.

At sufficient wind speed the aerodynamic uplift force and/or the overturning moment on the element may become higher than the weight and/or the resisting moment due to gravity or other restraints, such as strapping, and lift off will occur.

Interlocking and strapping systems are commonly used to improve the wind performance of roof pavers. In this case, the uplift force tends to be shared across several pavers. Fig. 2(b) shows a strapping system running transverse to the axis of the vortex which connects to the center of each paver. The lift on the paver AB is now restrained not only by the weight of the paver AB but also by at least part of the weight of the adjacent pavers, on which there is little if any lift. The lift on the paver AB that is needed to both lift paver AB and also cause the adjacent pavers to rotate so that their edges at A and B become airborne, but not the farther edges, is about double that needed to lift the unconnected paver (Irwin *et al.* 2012). The lift required to cause the farther edges also to become airborne is about 3 times that for the unconnected paver. These considerations, along with the assumption that lift on real pavers varies approximately as wind velocity squared, lead to the expectation that strapping in the direction transverse to the line of the vortex will increase the lift off speed by a factor of approximately $\sqrt{2} = 1.4$ to $\sqrt{3} = 1.7$ (Irwin *et al*. 2012). Aly *et al*. (2012) also showed that locking a group of pavers together can be very effective for preventing lift-off of pavers located in critical regions on the roof. They recommended using a locking system able to hold a group of at least 4x4 or 5x5 pavers together.

## 4. Experimental setup and testing protocol

A number of large-scale experiments were performed by the authors, and described in an earlier paper (Asghari Mooneghi *et al*. 2014, Mooneghi *et al.* 2014). In the work discussed in this paper, the same experimental setup was used for additional tests to facilitate the development of design guidelines. The experiments were performed in the 12-fan Wall of Wind (WOW) open jet facility at FIU which is able to generate hurricane winds up to Category 5 Saffir–Simpson Scale that replicate a representative mean wind speed profile and the high frequency end of the turbulence spectrum. A set of triangular spires and floor roughness elements was used to generate appropriate turbulence and boundary layer characteristics (Fig. 3).

Fig. 4 shows the comparison of longitudinal WOW spectrum and the Von Karman longitudinal spectrum at full scale using $L_u$=12 m and $I_u$=0.3 at 3.048 m height in suburban terrain (z0=0.2). It can be seen that there is a good match between the two spectra at high frequencies which has been noted by a number of previous researchers as necessary for correct simulation of local flow aerodynamics on low-rise buildings (Melbourne 1980, Saathoff and Melbourne 1997, Kumar and Stathopoulos 1998, Tieleman 2003, Richards *et al*. 2007, Yamada and Katsuchi 2008, Irwin 2009, Banks 2011, Kopp and Banks 2013). However, at low frequencies turbulence energy is missing. This is a common limitation when testing at large model scales, due to the limited size of wind tunnel working sections, but it can be largely overcome in post-test analysis using Partial Turbulence Simulation (PTS) theory based on quasi-steady assumptions as described by Asghari Mooneghi (2014) and Asghari Mooneghi *et al.* (2015).

(a) Inlet view

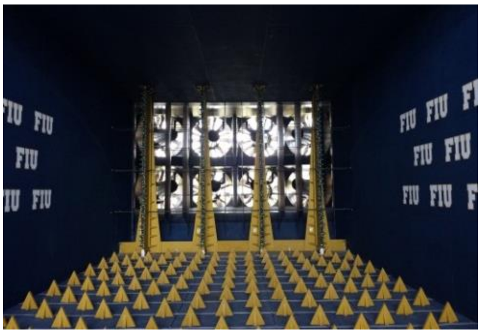

(b) Outlet view, Spires and floor roughness elements

Fig. 3 Wall of Wind, Florida International University

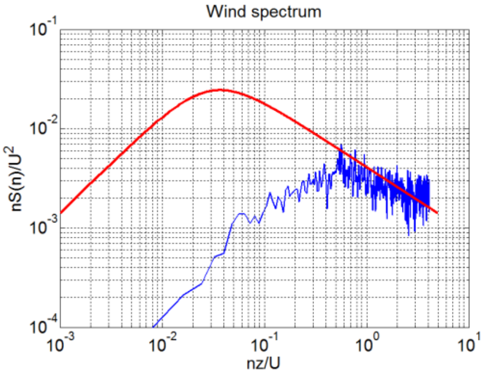


Fig. 4 Comparison of WOW Partial Spectrum and the Von Karman Spectrum at Full Scale

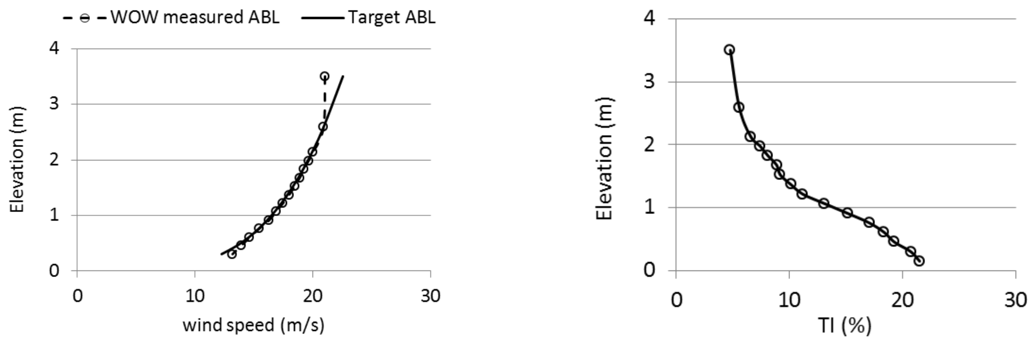


(a) Atmospheric Boundary Layer (ABL) profile (b) Turbulence intensity profile

Fig. 5 Simulated Suburban Terrain

The mean wind speed and turbulence intensity profiles for suburban terrain are shown in Fig. 5 for 20.1 m/s wind speed (target power law coefficient was $\alpha$=1/4).

The dynamic similarity requirements for the tests and how they were satisfied have been described by Asghari Mooneghi *et al.* (2014). The size of the 1:2 test building model was 3.35 m by 3.35 m in plan by 1.524 m high, representing at half scale a low-rise prototype building with height of 3.048 m. The size of the test section was 6.1 m wide and 4.3 m. high.

The test model height was around 35% of the wind field height generated by the WOW. This was within the 33% to 50% of the wind field height recommended by Aly *et al*. (2011) for obtaining roof pressure measurements with insignificant blockage effects in open jet facilities (Habte *et al*. 2015). The test model was located at a distance of around 13.70 m from the WOW fans, thus abiding by the minimum proximity requirement recommended by Bitsuamlak *et al*. (2010).

The roof deck was made from plywood and was completely sealed and rigid. The rectangular sharp edged parapets on the building model were interchangeable which allowed the parapet height to be adjusted. There were no parapets on the leeward side of the building. This was done with the intent that the model roof could be representative of the windward corner of a bigger roof structure on which the downwind parapets would not significantly influence flow over the upwind portions of the roof. Lin and Surry (1998) and Lin *et al*. (1995) showed that, for low buildings which are large enough to have reattached flows on the roof, the distribution of pressure coefficients in the corner region is mainly dependent on the eave height, *H*, and not so much on the building plan dimensions for similar terrain conditions. Moreover, external pressure coefficients measured in the wind tunnel by Kopp *et al.* (2005) on roof corners of a nearly flat building model were consistent with those measured on roof corners of flat roof low-rise building models with the same height but with different plan aspect ratios (Stathopoulos 1982, Stathopoulos and Baskaran 1988, Ho *et al.* 2005, Pierre *et al.* 2005).

Both wind blow-off testing (i.e., blowing at sufficient speed to dislodge pavers) and pressure measurements were performed. For the wind blow-off tests, concrete pavers with dimensions of 0.305 m by 0.305 m by 2.54 cm thickness with weight per unit area of 535 N/m$^2$ were installed on the roof which can be considered as modeling typical 0.61 m square pavers at half-scale (Fig. 6(a)). The pavers were numbered from 1 to 100 (Fig. 7(a)). For the pressure measurements, pavers with exactly the same dimensions as the concrete pavers (0.305 m × 0.305 m × 2.54 cm thickness) were made from Plexiglas which made it more convenient to install pressure taps on both upper and lower surfaces.

In order to study the effects of the pavers' edge gap to spacer height ratio, adjustable height pedestals were used to change the space between the pavers and the roof deck ($H_s$, Fig. 6(c)). A constant gap of G=3.175 mm at model scale (6.35 mm at full scale) between adjacent pavers (Fig. 6(c)) was maintained. Bienkiewicz and Endo (2009) carried out a wind tunnel study for studying the effects of the gap (G) between pavers, and the space ($H_s$) beneath the pavers on the pressures underside the loose-laid roof pavers. Results from these experiments showed that G reduced the underside pressure significantly but $H_s$ did not show clear tendencies. Instead, they introduced a parameter of the gap to spacer height ratio ($G/H_s$) and showed that this parameter controls the underside pressures, in a way that the higher the ratio, the less the net pressure on the pavers. Here the authors have adopted the same approach of using the $G/H_s$ ratio as the governing parameter. For very small gap sizes, Reynolds number effects could eventually make this assumption questionable but for the size of gap tested here (which is typical for most current paver systems) Reynolds number effects were expected to be minor.

A total of 13 experiments were carried out, including three wind blow-off tests and 10 pressure measurement tests. A summary of the parameters for each test is given in Table 1.

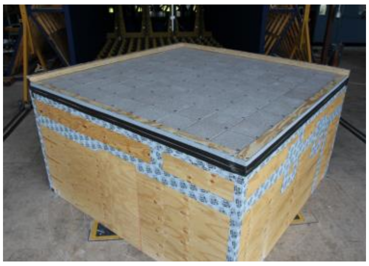

(a) Test building for wind blow-off tests

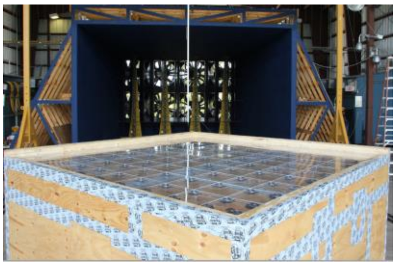

(b) Test building for pressure measurements

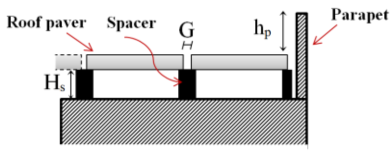


(c) Geometrical parameter definition

Fig. 6 Test setup configuration

Table 1 Test number and characteristics

| Test Number | $G/H_s$* | $(h_p/H)_{windward}$** |
|---|---|---|
| Wind Uplift 1 | 0.25 | 0.05 |
| Wind Uplift 2 | 0.083 | 0.05 |
| Wind Uplift 3 | 0.028 | 0.05 |
| Pressure 1-1 | 0.25 | 0.05 |
| Pressure 1-2 | 0.25 | 0.067 |
| Pressure 1-3 | 0.25 | 0.1 |
| Pressure 2-1 | 0.083 | 0.033 |
| Pressure 2-2 | 0.083 | 0.05 |
| Pressure 2-3 | 0.083 | 0.1 |
| Pressure 2-4 | 0.083 | 0.15 |
| Pressure 3-1 | 0.028 | 0 |
| Pressure 3-2 | 0.028 | 0.05 |
| Pressure 3-3 | 0.028 | 0.1 |

*Constant G=3.175 mm (at model scale) for all tests

** Parapet height was measured from top of the pavers. Leeward building sides did not have any parapet.

Table 2 Failure wind speed

| Test Number | Failure wind speed when wobbling of pavers started (m/s) | Failure wind speed when a couple of pavers lifted off from roof (m/s) |
|---|---|---|
| Wind Uplift 1 | 50 | 53.7 |
| Wind Uplift 2 | 45.7 | 50.1 |
| Wind Uplift 3 | 37.6 | 41.3 |

The test procedure consisted of first conducting wind lift-off tests to find out the location where paver lift-off first occurred so that the pressure tap layout for the pressure measurements could be concentrated on the most critical pavers. Only one wind direction was tested, a quartering direction of 45° relative to the roof edge. Based on past studies this wind direction was assessed to be the critical orientation for generating high paver uplift under conical vortices on flat rectangular roofs (Holmes 2015). Also, extensive experiments on roof pavers by Kind (1981) showed that, even though higher local roof suctions may occur for other directions, 45° is still the most critical direction for paver lift-off. Presumably this is due to the shape of the pressure distribution being less effective in lifting the pavers for other directions. The failure wind speeds measured at the roof height of the test model (1.524 m height) are reported in Table 2. These values are converted to full-scale values using Froude number scaling, i.e. full scale velocity $=\sqrt{2}\times$model velocity. The values reported in Table 2 are equivalent to 3s gust speeds at full scale. A summary of the method to calculate the equivalent 3s gust speeds is given in Appendix A.

The failure mechanism for the wind lift-off tests is explained in detail in the previous paper by the authors (Asghari Mooneghi *et al.* 2014). For pressure measurements, the original concrete pavers were replaced by the Plexiglas pavers with installed pressure taps (total of 447 pressure taps were used). The pressure tap layout is given in Fig. 7(b) for the exterior surface. The pressure tap layout for the underneath surface was about the same as the one given on the exterior surface with some minimal difference in the locations of pavers on the pedestals (Asghari Mooneghi *et al.* 2014). Nine critical pavers were fitted with a total of 256 pressure taps allowing accurate measurements to be made of the pressure distribution on the top and bottom surfaces.

Pressure measurements were carried out at a wind speed of 18.5 m/s which was below the failure speed of concrete pavers. A 512 channel Scanivalve Corporation pressure scanning system was used for pressure measurements. Pressure data were acquired at a sampling frequency of 512 Hz for a period of three minutes. Data were low-pass filtered at 30 Hz (equivalent to 21 Hz at full scale). A transfer function was used to correct for tubing effects in the post-test analysis (Irwin *et al.* 1979).

## 5. Experimental results and discussion

### 5.1 Aerodynamic pressure results

In this section the results from the pressure measurement experiments are discussed. The mean pressure coefficient at any location was obtained from

$$Cp_{mean} = \frac{(P-P_0)_{mean}}{\frac{1}{2}\rho U^2} \tag{1}$$

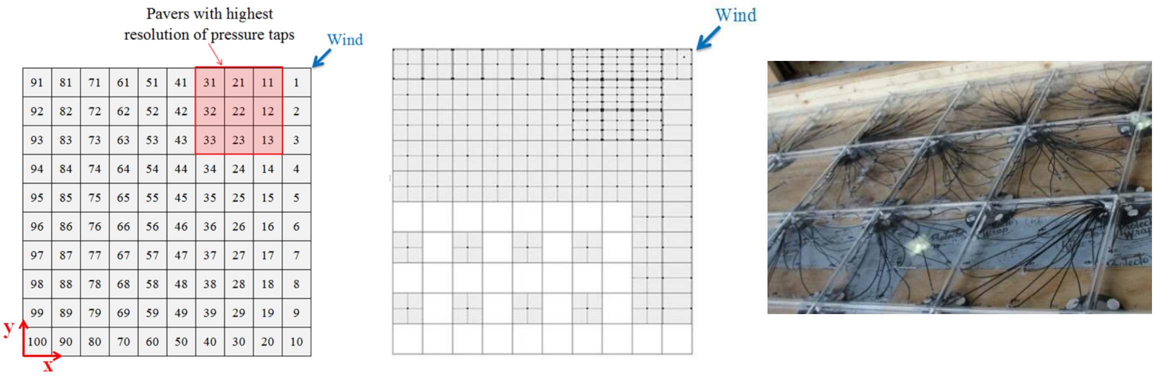


(a) Pavers numbering (b) External pressure tap layout (c) Critical pavers instrumented with pressure taps

Fig. 7 Details of the Experimental Setup where $P_{mean}$ is the mean pressure, $P_0$ is the static reference pressure, ρ is the air density at the time of the test (1.225 kg/m$^3$) and $U$ is the mean wind speed measured at the building height of the test model (1.524 m). The peak pressure coefficient was obtained from:

$$Cp_{peak} = \frac{(P-P_0)_{peak}}{\frac{1}{2}\rho U_{3s}^2} \tag{2}$$

where $P_{peak}$ is the peak pressure, and $U_{3s}$ is the peak 3-s gust speed at the reference height. The tests were performed in partial turbulence simulation, hence the turbulence intensity at roof height was lower than that of atmospheric boundary layer (ABL) which contains full spectrum of turbulence. In order to calculate the peak pressure, $P_{peak}$, a method called "Partial Turbulence Simulation" (PTS) was used. In this method, the turbulence is divided into two distinct statistical processes, one at high frequencies which can be simulated correctly in WOW, and one at low frequencies which can be treated in a quasi-steady manner. The joint probability of load from the two processes is derived, with one part coming from the WOW data and the remainder from the Gaussian behavior of the missing low frequency component. The PTS method is discussed in details in Asghari Mooneghi (2014). It should be noted that in this method, the $Cp_{peak}$ is first calculated based on mean hourly dynamic pressure, that would have been obtained had the full spectrum been present which can then be converted to $Cp_{peak}$ based on gust pressure corresponding to any selected gust duration, e.g., 3 seconds. For the current test configuration, $U_{3600sec}/U_{3sec} = 1.8$ was used. This factor was calculated for suburban terrain at z=3.048 m. The procedure for converting the wind speed averaging time was based on Harris and Deaves (1981) model taken from ESDU (1985). For the evaluation of these estimated values, the peak value with 85% probability of not being exceeded in one hour of full spectrum wind was selected (Asghari Mooneghi 2014). The choice of the 85% probability of non-exceedance for obtaining the peak pressure coefficients is not materially very different from the 80% recommendation of the ISO 4354 standard (International Standard 2009).

The net total pressure coefficient, defined as the instantaneous difference between the external and the corresponding underneath pressure coefficient at the same location, is

$$Cp_{net}(t) = Cp_{ext}(t) - Cp_{int}(t) \tag{3}$$

Mean and peak external pressure coefficients, mean underneath pressure coefficient and net mean pressure coefficients contours for the case of $G/H_s$=0.028 and $h_p/H$=0 (i.e., no parapet case) are given in Fig. 8.

The results of the tests show that pavers close to the edges and corners of the roof are subjected to the highest local negative pressures. These areas are under the conical vortices. As compared to external pressures the underneath pressures are lower in magnitude and show more uniformity. Pressure equalization reduces the net uplift force on the pavers. It should be noted that the peak values correspond to the estimated peak values for each tap during the test and do not happen simultaneously on all taps. In all tests, paver 21 was shown to be the most critical paver. So, in the rest of the paper, results are calculated for this paver.

The overall wind lift load, $L(t)$, acting on any single paver and the lift coefficient $C_L(t)$ are obtained as

$$L(t) = \frac{1}{2}\rho U^2 \iint_{A_{paver}} Cp_{net}(t)dA \tag{4}$$

$$C_L(t) = \frac{L(t)}{\frac{1}{2}\rho U^2 A} \tag{5}$$

where $A$ is the surface area of the paver. It should be noted that the highest suction on the paver does not necessarily occur at the center of the paver. This means that even for cases where the total uplift force is less than the weight of the paver, the weight of the paver might not overcome the corresponding overturning moment from the wind suction forces. The overturning moment about a selected axis and the moment coefficient $C_M(t)$ can be obtained from

$$M(t) = \frac{1}{2}\rho U^2 \iint_{A_{paver}} Cp_{net}(t) \times d \times dA \tag{6}$$

$$C_M(t) = \frac{M(t)}{\frac{1}{2}\rho U^2 A a} \tag{7}$$

where $d$ is the moment arm defined as the distance from a selected axis to each point on the paver (Fig. 9).

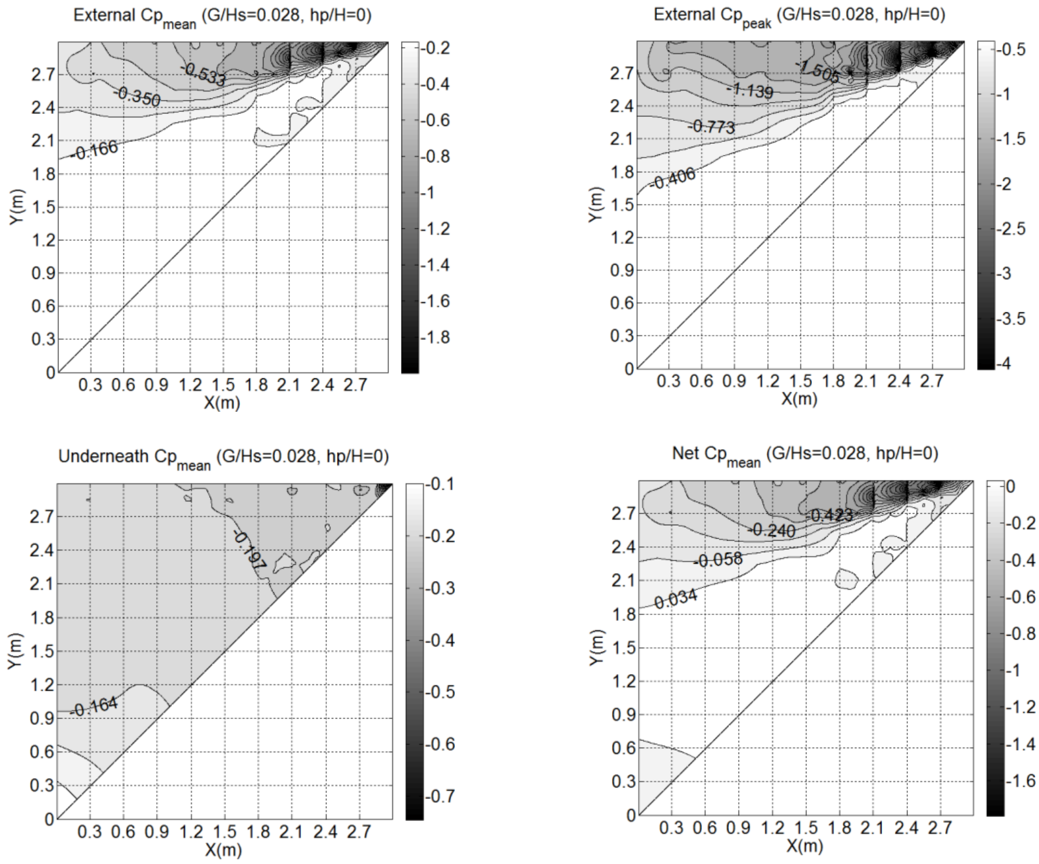


Fig. 8 Pressure coefficient contours ($G/H_s$=0.028 and $h_p/H$=0)

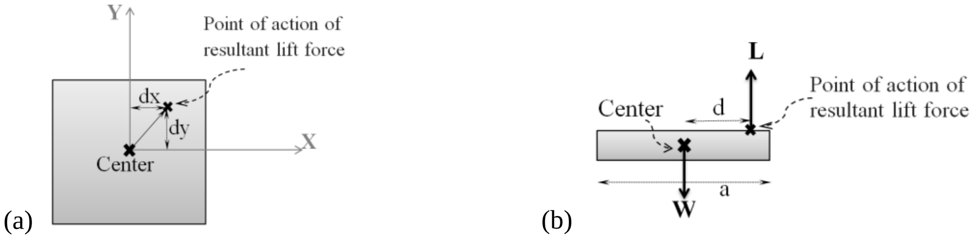


Fig. 9 Definition of the point of action of the resultant lift force: (a) plan view and (b) side view

Table 3 shows the variations of the most negative mean and peak local $C_{p,ext}$ values, $C_{Lext}$, $C_{Lnet}$, $C_{Mx,net}$ and $C_{My,net}$ on paver 21. Fig. 10 shows highest local suction coefficients for various $G/H_s$ and $h_p/H$ ratios. The $G/H_s$ ratio affects the underside pressures such that the higher the ratio, the less the net pressure on the pavers.

The highest external single tap pressure coefficients and the external area averaged pressure coefficient ($C_{Lext}$) observed on the most critical paver (paver 21) obtained for different cases (Table 3) were compared to component and cladding external pressure coefficients for roofs as given in ASCE 7-10. For gable roofs with slope $\theta \leq 7^o$ the largest external pressure coefficient for corner Zone 3 for tributary areas less than 0.9 $m^2$ is given as -2.8 in Fig. 30.4-2A (ASCE 7-10).

Table 3 $C_{p,ext}$, $C_{Lext}$, $C_{Lnet}$, $C_{Mx,net}$ and $C_{My,net}$ on paver 21

| Test case | | Highest $C_{p,ext}$ read on a tap (paver 21) | | $C_{Lext}$ | | $C_{Lnet}$ | | $C_{Mx,net}$ | | $C_{My,net}$ | |
|---|---|---|---|---|---|---|---|---|---|---|---|
| **$G/H_s$** | **$h_p/H$** | **Mean** | **Peak** | **Mean** | **Peak** | **Mean** | **Peak** | **Mean** | **Peak** | **Mean** | **Peak** |
| **0.25** | 0.05 | -1.70 | -3.14 | -0.89 | -1.38 | -0.44 | -0.80 | -0.02 | -0.10 | -0.02 | -0.08 |
| **0.25** | 0.067 | -1.44 | -2.92 | -0.90 | -1.41 | -0.44 | -0.80 | 0.00 | -0.10 | -0.03 | -0.08 |
| **0.25** | 0.1 | -1.45 | -2.43 | -0.96 | -1.39 | -0.39 | -0.77 | 0.01 | -0.06 | -0.02 | -0.08 |
| **0.083** | 0.033 | -1.68 | -2.88 | -0.86 | -1.30 | -0.57 | -0.96 | -0.02 | -0.10 | -0.03 | -0.08 |
| **0.083** | 0.05 | -1.71 | -2.71 | -0.89 | -1.35 | -0.60 | -1.01 | -0.01 | -0.09 | -0.03 | -0.09 |
| **0.083** | 0.1 | -1.60 | -2.44 | -0.98 | -1.43 | -0.59 | -0.99 | 0.02 | -0.07 | -0.03 | -0.09 |
| **0.083** | 0.15 | -1.31 | -2.05 | -0.91 | -1.26 | -0.47 | -0.81 | 0.01 | -0.02 | -0.02 | -0.07 |
| **0.028** | 0 | -1.20 | -4.10 | -0.70 | -1.19 | -0.52 | -0.98 | -0.06 | -0.15 | -0.01 | -0.10 |
| **0.028** | 0.05 | -1.86 | -2.85 | -0.97 | -1.44 | -0.75 | -1.20 | -0.01 | -0.09 | -0.03 | -0.10 |
| **0.028** | 0.1 | -1.53 | -2.50 | -0.99 | -1.40 | -0.74 | -1.14 | 0.02 | -0.06 | -0.04 | -0.09 |

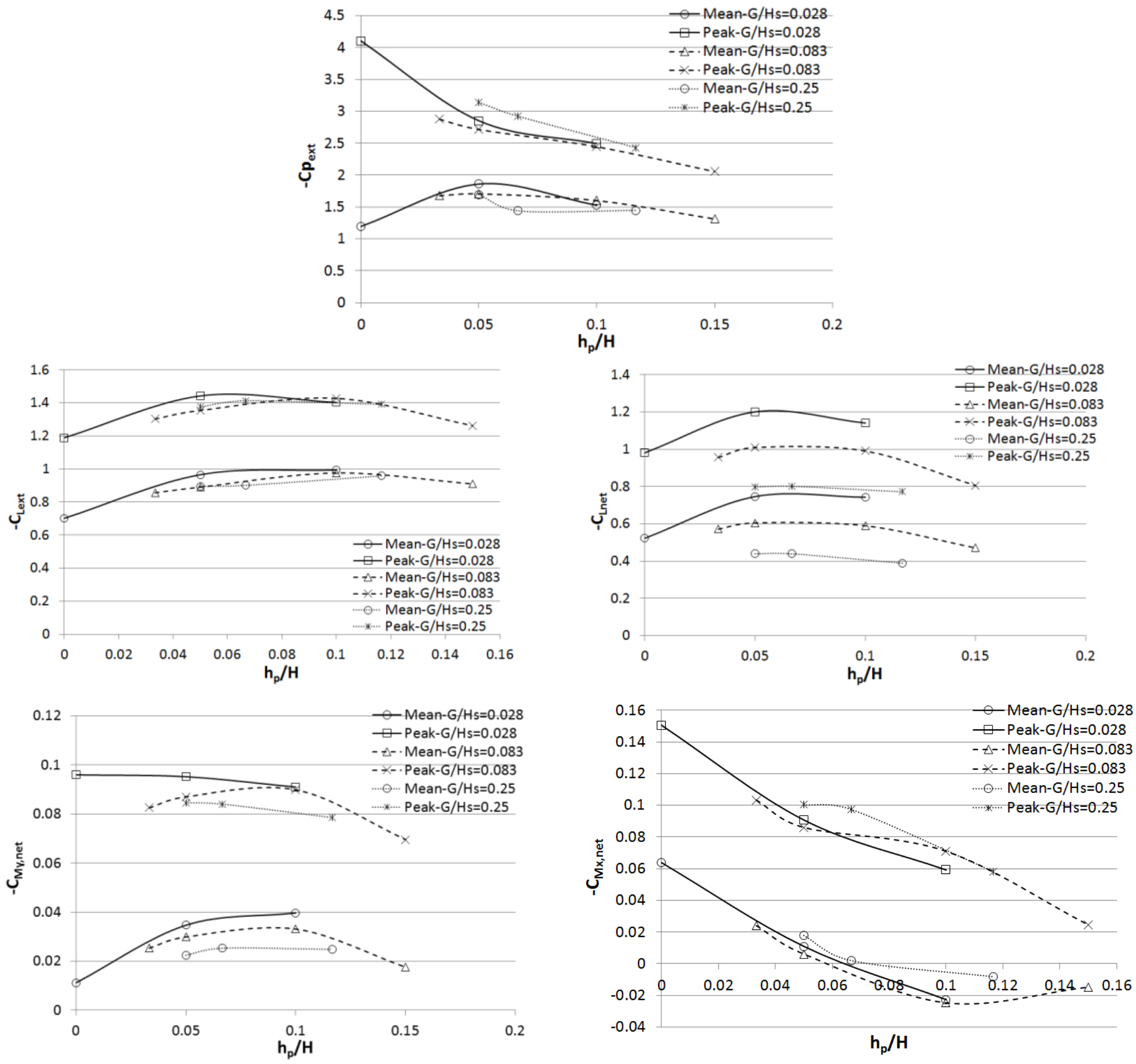


Fig. 10 Highest local suction coefficients on the roof $C_{Lext}$, $C_{Lnet}$, $C_{Mx,net}$ and $C_{My,net}$ on paver 21

The highest single tap peak suction coefficients observed in the present tests for all cases ranged from -4.1 for $h_p/H=0$ and $G/H_s=0.028$ to -2.05 for $h_p/H=0.15$ and $G/H_s=0.083$ in the critical paver zone. The highest peak external lift coefficients ranged from -1.44 for $h_p/H=0.05$ and $G/H_s=0.028$ to -1.19 for $h_p/H=0$ and $G/H_s=0.028$. The underneath pressure coefficients required for calculating the net pressure coefficients are not dealt with in ASCE 7-10.

The reduction in the net wind uplift can be expressed as

$$r = \frac{C_{Lnet}}{C_{Lext}} \tag{8}$$

The reduction factor defined as the ratio of the net lift coefficient to the external lift coefficient is plotted as a function of relative parapet height ($h_p/H$) for different $G/H_s$ for paver 21 (Fig. 11).

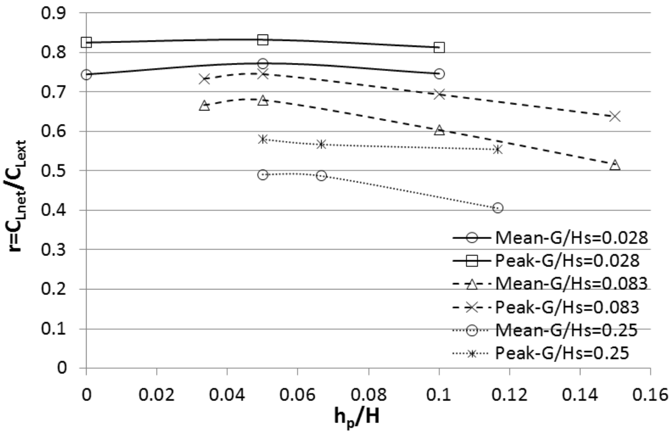


Fig. 11 Reduction factor $r = C_{L_{net}}/C_{L_{ext}}$

The results show that increasing the $G/H_s$ ratio decreases the reduction factor. This means that the correlation between upper and lower surface pressures decreases with decreasing the $G/H_s$ ratio. Thus, increasing the ratio of the pavers' edge-gap to spacer height can reduce the net wind-induced uplift loading on the pavers and improve the performance of the pavers. The reduction factor is not very sensitive to parapet height for $h_p/H$ less than about 0.1. For $h_p/H$ ratios beyond 0.1 the reduction factor reduces gradually, i.e., improved performance of the pavers can be expected.

### *5.2 Effect of connecting pavers*

There are various types of interlocking and strapping systems available to improve the wind performance of roof paving systems. The effect of a specific system has not been dealt with during the experiments in this study. However, guidance on the effectiveness of these systems can be obtained by evaluating the net uplift on groups of pavers rather than only one. The $C_{L_{net}}$ value is calculated for 6 different cases shown in Fig. 12 and compared to the highest $C_{L_{net}}$ value observed during the experiments on Paver 21 (Fig. 13). In Fig. 12, the highlighted pavers were assumed to act as a single unit for the case of $G/H_s$=0.083 and $h_p/H$=0.05. The most critical paver is shown with an X mark.

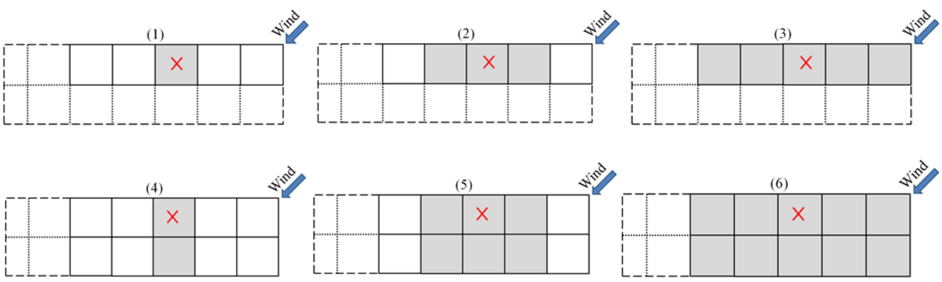


Fig. 12 Interlocked pavers in different configurations

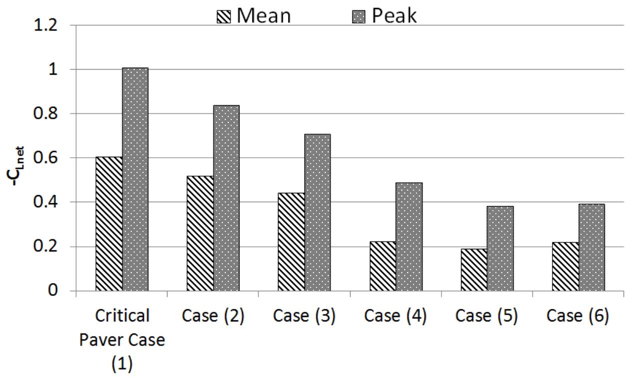


Fig. 13 Comparison between $C_{L_{net}}$ values for different configurations defined in Fig. 12

The results illustrate the effect of connecting pavers together in reducing the net uplift force on the linked pavers as a unit. Based on the characteristics of the strapping or interlocking system in hand, different degrees of improvement can be expected. It should be noted that the surface pressure variation along the axis of the vortex varies much more slowly than in the transverse direction. So, strapping in the direction roughly parallel to the axis of the vortex is not expected to be as effective in restraining pavers from lift off as strapping in the transverse direction. If there is a high uplift on one paver the adjacent pavers in the direction along the vortex axis are likely to also experience significant uplift. Real strapping systems rarely align directly with the vortex axis or transverse to it. Therefore strapping in both orthogonal directions of a paving system is preferable.

### *5.3 Comparison of the results from pressure measurement experiments with wind lift-off tests*

In this section the critical wind velocities for pavers' lift-off are calculated from the pressure measurement results and are compared to the results obtained from the wind lift-off tests. This is done to verify that the wind lift-off speeds that were calculated from the pressure measurements were in accord with the blow off tests. Lift-off takes place when the moment caused by the uplift force equals (or just exceeds) the resisting moment from the paver weight, $W$. Therefore, the critical wind velocity $U_{CRIT}$ at which lift-off occurs is calculated from Eq. (10) in which the moment is taken about the edge of the paver.

$$\frac{1}{2}\rho U_{CRIT}{}^{2} C_L A\left(d+\frac{a}{2}\right) = W \times \frac{a}{2} \tag{9}$$

$$U_{CRIT} = \sqrt{\frac{a}{2\left(d+\frac{a}{2}\right)} \times \frac{W}{\frac{1}{2}\rho C_L A}} \tag{10}$$

where $C_L$ is the lift coefficient obtained from the pressure measurement results and $a$ and $d$ are defined in Fig. 9. Fig.14 shows the critical wind lift-off speeds obtained from wind lift-off tests (Table 2) as compared to the critical wind lift-off speeds calculated from Eq. (10) using the pressure measurement results. The wind speeds presented in Fig. 14 are the equivalent 3-sec gust speed.

For the limiting case of $G/H_s$ ~ zero (meaning a very large spacer height for a specific edge-gap between the pavers) one can assume that the underneath pressure needed would be similar to the internal pressure inside a building with a porous roof. The underneath pressure coefficient for this case is calculated as the average of external pressure coefficients recorded at the center of all pavers using

$$C_{p_{int}}(t) = \frac{1}{N}\left(\sum_{i=1}^{n=N} C_p(t)_{ext}\,|_{center\ of\ paver\ i}\right) \tag{11}$$

where N is the total number of pavers. The net lift coefficient was then calculated using

$$C_{L_{net}}(t) = C_{L_{ext,on\ paver\ 21}}(t) - C_{L_{int}}(t) \tag{12}$$

It is not known in advance what averaging time for wind load the pavers react to except by hypothesizing various values and seeing what lines up best with the lift-off test results. Therefore the lift-off speeds from pressure measurements presented in Fig. 14 were calculated once based on the mean $C_{Lnet}$ and once based on peak $C_{Lnet}$. The results showed that wobbling of the pavers started at slightly lower speed than would be predicted purely on the basis of the mean $C_{Lnet}$ value combined with 3 second gust speed. This implies that some of the high frequency gust action occurring at shorter duration than 3 seconds was also necessary to initiate wobbling. However, assuming that the full gust speed is required to start wobbling of the pavers would be on the conservative side. The results show that beyond a certain value of Hs (i.e., for small $G/H_s$ values) the pressures on the underneath can communicate very rapidly with other parts of the roof and further increases in $H_s$ do not make much difference. Once this point is reached there are no further decreases in lift-off velocity. The point where this situation is reached is around $G/H_s$ ~ 0.03 ($H_s/G$ ~ 30).

### *5.4 Comparison of the critical wind lift-off speeds from experiments with those obtained from studies based on ASCE 7-10 pressure coefficients*

The design wind pressures on buildings in the United States are determined using the ASCE 7-10 standard. It provides wind loads for the design of the Main Wind Force Resisting System (MWFRS), as well as Components and Cladding. These provisions cover buildings with common shapes, such as those with Flat, Gable, Hip, and Mono-slope roofs, under simple surrounding conditions. For the design of roof components and cladding, the roof is divided into rectangular shaped zones within which a constant pressure coefficient is specified. For permeable roof claddings such as loose-laid roof pavers, the ASCE standard currently does not provide specific guidance for estimating net wind uplift loads. Two methods were examined in this paper for estimating the critical wind lift-off speeds from the exterior pressure coefficients given in ASCE 7-10 as follows

Case I: A practice proposed for roof tiles (Florida Public Hurricane Loss Projection Model (FPHLPM), 2005, Volume II, p. 55) is to assume a zero underneath pressure coefficient and consider the exterior pressure coefficient as the net pressure coefficient. The critical lift of speed can then be calculated using

$$U_{CRIT} = \sqrt{\frac{W}{\frac{1}{2}\rho C_{p_{ext}} A}} \tag{13}$$

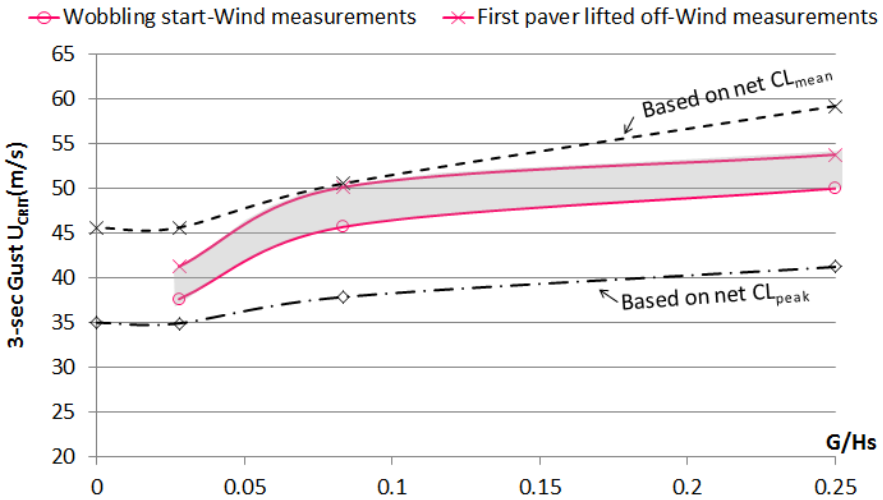


Fig. 14 Comparison between wind lift-off speeds from wind blow-off tests and those obtained from pressure measurements

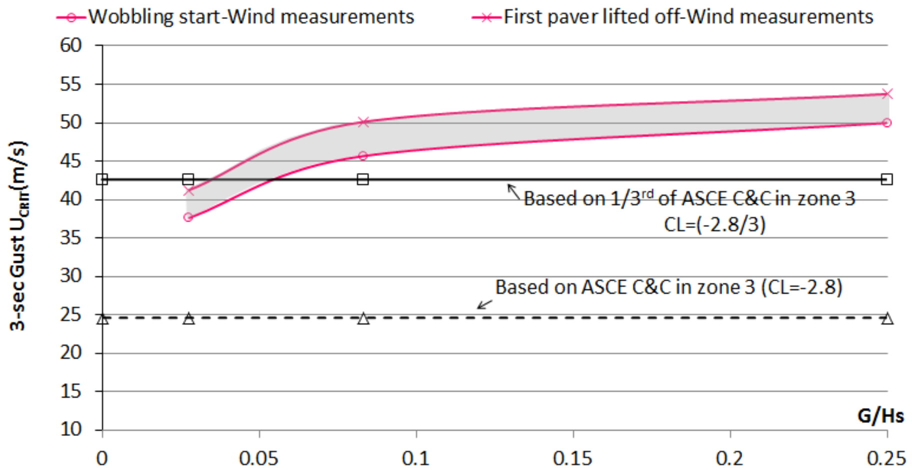


Fig. 15 Comparison between wind lift-off speeds from wind blow-off tests and those obtained from a typical practice based on ASCE 7-10 exterior pressures on C&C and 1/3$^{rd}$ Rule

Fig. 15 shows a comparison of this approach with the lift off speeds from the current experiments. For the estimates based on ASCE 7-10 exterior pressures, the wind blow-off speeds were calculated using GCp=-2.8 (external pressure coefficient in Zone 3 for $A_{eff}$=0.09 m$^2$ $\leq$ 0.93 m$^2$). In Fig. 15 the critical wind blow-off speed calculated based on this approach is clearly very conservative. This emphasizes the need for better guidelines.

Case II: In Building Research Establishment (1985) it is stated that the magnitude of the net uplift coefficient was found empirically to be generally less than 1/3$^{rd}$ of the magnitude of the peak negative external pressure coefficient on the upper surface of the paver. In other words as a rule of thumb, $C_L \leq -\frac{1}{3}Cp_{peak}$. This is broadly in line with earlier findings of Kind and Wardlaw (1982). Therefore, 1/3rd of the ASCE 7-10 exterior pressure coefficients for components and claddings was used to estimate the critical wind lift-off speed (Eq. (13)) and results are also shown in Fig. 15. This approach, called here the $1/3^{rd}$ Rule, can be seen from Fig. 15 to over predict the wind lift-off speeds for lower $G/H_s$ ratios and under predict them at higher $G/H_s$ ratios. The design guidelines presented in Section 6 of this paper do take into account the effects of different $G/H_s$ ratios, thereby improving on the simple $1/3^{rd}$ rule.

## 6. Design guidelines for roof pavers

Based on the results presented in the previous sections, the following equation is proposed for the design of loose-laid roof pavers

$$C_{L_{net}} = R_1 \times R_2 \times Cp_{ASCE\ 7-10,exterior,C\&C,Zone\ 3} \tag{14}$$

where $R_1$ is a reduction factor for different gap ratios and $R_2$ is a reduction factor for different parapet heights. These are to be applied to the ASCE 7-10 exterior pressure coefficients for components and claddings in Zone 3. Here, Zone 3 in ASCE 7-10 is chosen as the worst case scenario for design of roof pavers. However, $R_1$ in Eq. (14) can be modified to take into account the effects of location on the roof. Failure is defined here as the start of wobbling. $R_1$ and $R_2$ are to be calculated from the diagrams proposed in the following. The equivalent uplift force can then be calculated by multiplying Eq. (14) by the dynamic pressure at roof height.

### *6.1 $R_1$ reduction factor: Effect of $G/H_s$ ratio*

The $R_1$ reduction factor is defined as $C_{L_{net}}/C_{p_{ext}}$ in which $C_{p_{ext}}$ is the ASCE 7-10 exterior pressure coefficient for components and cladding in Zone 3 and $C_{L_{net}}$ values were calculated using the following formula in which failure is assumed to occur with the start of wobbling.

$$U = \sqrt{\frac{W}{\frac{1}{2}\rho C_L A}} \rightarrow C_{L_{estimated}} = \frac{(W/A)}{\frac{1}{2}\rho U^2{}_{CRIT(wobbling\ start\ from\ wind\ tests)}} \tag{15}$$

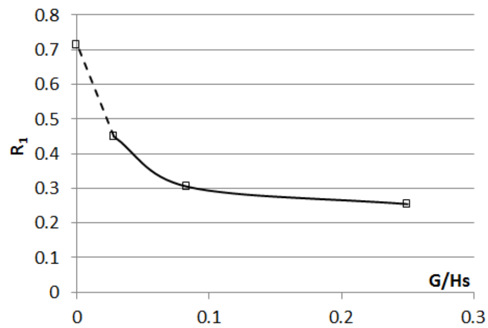


Fig. 16 $R_1$ reduction factor for different $G/H_s$ ratios

The proposed reduction factor $R_1$ based on G/$H_s$ ratio is plotted in Fig. 16. The value at G/$H_s$ ~ 0 comes from assuming $C_{L_{net}} = -2$ in which $C_{L_{ext}}$ is assumed to be -2.8 and $C_{L_{int}} = -0.8$ which is approximately calculated from averaging the external peak pressure coefficients on pavers 11, 12, 21, 22, 31, and 32. The $R_1$ factor changes an exterior local peak pressure coefficient into a net lift coefficient taking into account the pressure distribution over the paver and the effect of G/$H_s$ on pressure equalization.

### *6.2 $R_2$ reduction factor: Effect of parapet height*

$R_2$ reduction factor is proposed based on results presented in Fig. 11. For relative parapet height ratios less than 0.1 no reduction in the $C_L$ value is proposed (i.e., $R_2 = 1$). In ASCE 7-10 Figure 30.4-2A it is stated that the external pressure coefficients for Zone 3 can be reduced to the values in Zone 2 for parapets higher that 0.9144 m. (3 ft.). This means about 36% reduction for $h_p$/H ratio of 0.3 and higher for the current experimental setup. This value is considered as the upper limit of the proposed reduction proposed in Fig. 17 (i.e., $h_p$/H=0.3). Kind *et al.* (1987) proposed $h_p$/H =0.1, $h_p$/H =0.02 and $h_p$/H =0.03 for low, mid and high-rise buildings respectively, above which a somewhat rapid reduction in the worst suction values due to the parapet was observed. This would imply that application of the reduction factor in Fig. 17 to mid and high-rise buildings would be conservative.

In Fig. 18 the proposed curve in Fig. 17 for $R_2$ reduction factor is compared to the experimental results presented previously in Fig. 11. The solid and dashed lines are plotted by applying respectively the $R_2$ factor to the maximum of peak and mean reduction factor $r = C_{L_{net}}/C_{L_{ext}}$ obtained from experiments (given in Fig. 11). This was done to make comparisons possible between the curves since due to pressure equalization effects, the experimental reduction factor $r = C_{L_{net}}/C_{L_{ext}}$ curves do not start at one as is the case for proposed $R_2$ reduction factor. The results show a good degree of agreement. In some cases (e.g. left graph in Fig. 18) the reduction due to parapet height from experiments ($r = C_{L_{net}}/C_{L_{ext}}$) might start at $h_p$/H ratios lower that the assumed $h_p$/H=0.1.

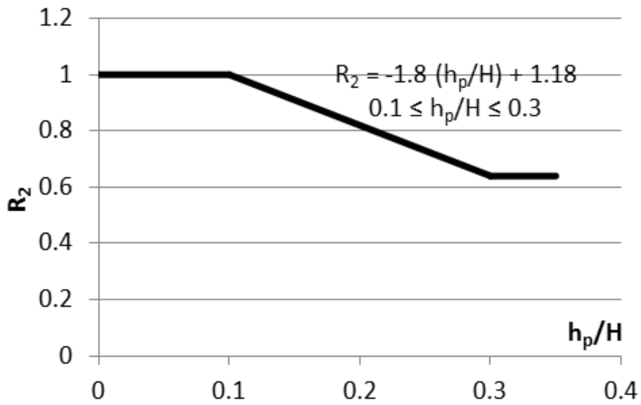


Fig. 17 $R_2$ reduction factor for different $h_p$/H ratios

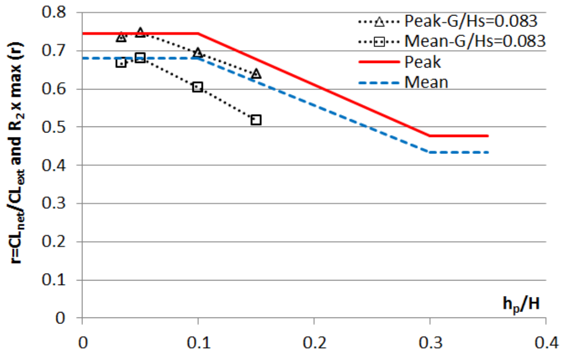


(a) G/H$_s$=0.083

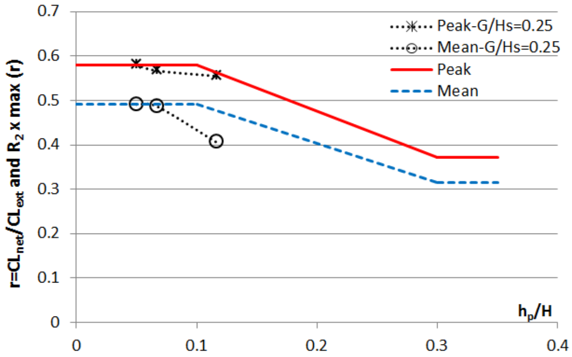


(b) G/H$_s$=0.25

Fig. 18 Comparison of proposed $R_2$ curve with r as a function of h$_p$/H

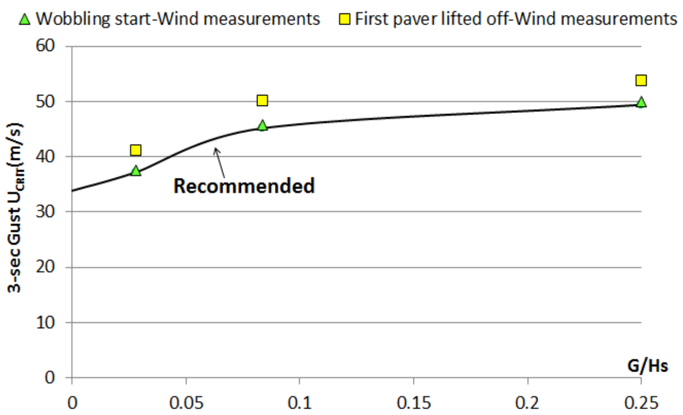


Fig. 19 Critical wind speed vs. G/H$_s$ (h$_p$/H=0.05 for wind measurements)

However, h$_p$/H=0.1 and the corresponding curve proposed in Fig. 18 are based on results obtained from multiple experiments in order to have a universal curve. The h$_p$/H=0.1 value is also obtained from the experiments of Kind et al. (1987). It should be noted that the rate of decrease of reduction factor $r = C_{L\,net}/C_{L\,ext}$ versus h$_p$/H (slope of the diagram between h$_p$/H=0.1 to h$_p$/H=0.3) obtained from experiments is in good agreement with that of proposed $R_2$ curve (Fig. 18).

Fig. 19 shows the critical lift-off speeds from the measurements compared to values from the proposed guideline.

### 6.3 Applications and special notes

1. The proposed guidelines were derived assuming a full scale paver size of 0.61 m by 0.61 m by 5.05 cm thickness. This particular size was selected as it represents a very common paver size on typical flat roof low-rise buildings used in the United States. The guidelines will work best for pavers that have sizes close to the size tested. Future experiments are

needed to investigate the applicability of the proposed guidelines for pavers with sizes and aspect ratios very different from the ones tested for the current work.

2. The effect of building height has not been examined in this paper. The building in the current experiments was a representative of a low-rise building. Based on the wind lift-off experiments performed by Kind *et al.* (1987) on the failure wind speeds for roof pavers on low-rise, mid-rise and high-rise buildings, the results presented in this paper are expected to be conservative when applied to mid and high-rise buildings provided the increase in roof height wind speed with building height is accounted for. However, further experiments are needed to fully quantify the effects of building height for mid and high-rise buildings.
3. The effect of paver size and geometry has not been evaluated in this paper. It is to be noted that the element size have an effect on the failure of non-interlocking roof pavers (Kind *et al.* 1987). Previous studies by Bienkiewicz and Sun (1997) indicated that square pavers are more wind-resistant than rectangular pavers.
4. The general effect of interlocking and strapping systems was investigated in this paper through the effect of load sharing mechanism between pavers. These systems are usually effective and improve the wind performance of roof pavers. The application of the proposed guidelines is primarily for loose-laid roof pavers without any interlocking or strapping system. However, some guidance of the effective reduction in lift-off forces can be drawn from the results in Figs. 12 and 13. For more precise results it is recommended to perform wind tunnel testing at large scale or full scale to find out the characteristics and wind performance of a specific interlocking or strapping system.
5. The experiments were performed in a simulated suburban terrain. The effect of wind turbulence was not examined in this paper but provided the 3 second gust speed is used to estimate lift-off the effects of different turbulence levels should be reasonably well accounted for.
6. The effect of thickness of the pavers on resistance to flow through the gaps between pavers was not examined in this paper. Increased thickness for the same gap might be expected to increase resistance to flow, thereby having a similar effect to reducing the gap. This is an area for further research.
7. It should be noted that the developed design guidelines are intended for use with the external pressure coefficients given in ASCE7-10 for components and claddings in zone 3. Caution should be exercised in using the proposed reduction factors in conjunction with external pressure coefficients given in other codes and standards.

## 7. Conclusions

The objective of this paper was to develop simple guidance in code format for design of commonly used loose-laid roof pavers. A set of 1:2 scale experiments was performed to investigate the wind loading on concrete roof pavers on the flat roof of a low-rise building. The experiments were performed in the Wall of Wind (WOW) hurricane testing facility at Florida International University (FIU). Experiments included both wind blow-off tests and detailed pressure measurements on the top and bottom surfaces of the pavers. Several conclusions were drawn:

- The paver's edge-gap to spacer height ratio affects the underside pressures such that the higher the ratio, the less the net uplift pressure on the paver. This may be regarded as increasing the failure wind speed.
- The relative parapet height, defined as the ratio of the parapet height to the building height, affects the failure wind speed. For very low-height parapets ($\sim h_p/H<0.1$), a small reduction in the failure wind speed was observed as compared to zero-height parapet. However, for taller parapets, increasing the parapet height results in an increased failure wind speed.
- The general effect of interlocking and strapping systems was studied through the effect of the load sharing mechanism between pavers. Interlocking and strapping systems improve the wind performance of the roof pavers since the uplift loads tend to be shared across several pavers.

Based on the experimental results and review of literature, guidelines are proposed for designing loose-laid roof pavers against wind uplift. The guidelines have been formatted so that use can be made of the existing information in codes and standards such as ASCE 7-10 on exterior pressures on components and cladding. The effects of pressure equalization, the paver's edge-gap to spacer height ratio and parapet height as a fraction of building height on the wind performance of roof pavers were investigated and are included in the guidelines as adjustment factors. The applications and limitations of the guidelines are discussed.

## Acknowledgments

We would like to greatly thank the Tile Tech Company for providing us with concrete roof pavers and the pedestal system required for the wind destructive tests. This research was supported by the National Science Foundation (NSF) (NSF Award No. CMMI-1151003) and the Florida Division of Emergency Management (DEM). The instrumentation was supported by NSF MRI Award (No. 0923365). The help received from our research assistant, Ramtin Kargarmoakhar is gratefully acknowledged. The help offered by the Wall of Wind manager, Walter Conklin and the Research scientists, Roy Liu Marquis and James Erwin is also greatly appreciated.

## References

Aly, A., Gan Chowdhury, A. and Bitsuamlak, G. (2011), "Wind profile management and blockage assessment for a new 12-fan Wall of Wind facility at FIU", *Wind Struct*., **14**(4), 285-300.

Aly, A.M., Bitsuamlak, G.T. and Chowdhury, A.G. (2012), "Full-scale aerodynamic testing of a loose concrete roof paver system", *Eng. Struct.*, **44**, 260-270.

Amano, T., Fujii, K. and Tazaki, S. (1988), "Wind loads on permeable roof-blocks in roof insulation systems", *J. Wind Eng. Ind. Aerod.*, **29**, 39-48.

AS 1170.2 (2011), *Australian/New Zealand standard: structural design actions*, Standards Australia/Standards New Zealand, Sydney, Australia.

ASCE 7-10 (2010), *Minimum Design Loads for Buildings and Other Structures*, American Society of Civil Engineers, ASCE, Virginia.

Asghari Mooneghi, M. (2014), *Experimental and Analytical Methodologies for Predicting Peak Loads on Building Envelopes and Roofing Systems*, FIU Electronic Theses and Dissertations, Paper 1846. http://digitalcommons.fiu.edu/etd/1846.

Asghari Mooneghi, M., Irwin, P. and Gan Chowdhury, A. (2014), "Large-scale testing on wind uplift of roof pavers", *J. Wind Eng. Ind. Aerod*., **128**, 22-36.

Asghari Mooneghi, M., Irwin, P. and Gan Chowdhury, A. (2015), "Partial Turbulence Simulation Method for Small Structures", *Proceedings of the14th International Conference on Wind Engineering*, Porto Alegre, Brazil, June.

Banks, D. (2011), "Measuring peak wind loads on solar power assemblies", *Proceedings of the 13th International Conference on Wind Engineering*, Amsterdam, Netherlands, July.

Banks, D., Meroney, R.N., Sarkar, P.P., Zhao, Z. and Wu, F. (2000), "Flow visualization of conical vortices on flat roofs with simultaneous surface pressure measurement", *J. Wind Eng. Ind. Aerod.*, **84**(1), 65-85.

Bienkiewicz, B. and Endo, M. (2009), "Wind considerations for loose-laid and photovoltaic roofing systems", *Proceedings of the Structures Congress*, Austin, Texas, April-May.

Bienkiewicz, B. and Meroney, R.N. (1988), "Wind effects on roof ballast pavers", *Eng. Struct.*, **114**(6), 1250-1267.

Bienkiewicz, B. and Sun, Y. (1992), "Wind-tunnel study of wind loading on loose-laid roofing system", *J. Wind Eng. Ind. Aerod.*, **43**(1-3), 1817-1828.

Bienkiewicz, B. and Sun, Y. (1997), "Wind loading and resistance of loose-laid roof paver systems", *J. Wind Eng. Ind. Aerod.*, **72**, 401-410.

Bitsuamlak, G., Dagnew, A. and Gan Chowdhury, A. (2010), "Computational assessment of blockage and wind simulator proximity effects for a new full-scale testing facilit", *Wind Struct.*, **13**, 21-36.

Bitsuamlak, G.T., Gan Chowdhury, A. and Sambare, D. (2009), "Application of a full-scale testing facility for assessing wind-driven-rain intrusion", *Build. Environ*., **44**(12), 2430-2441.

Bofah, K.K., Gerhardt, H.J. and Kramer, C. (1996), "Calculations of pressure equilibration underneath loose-laid, flow permeable roof insulation boards", *J. Wind Eng. Ind. Aerod.*, **59**(1), 23-37.

Building Research Establishment (1985), *Digest 295: Stability under wind load of loose-laid external roof insulation boards*, Building Research Station, Garston, Watford, UK.

Cheung, J.C.K. and Melbourne, W.H. (1986), "Wind loads on porous cladding", *Proceedings of the 9th Australasian Fluid Mechanics conference*, Auckland, New Zealand, December.

Cheung, J.C.K. and Melbourne, W.H. (1988), "Wind loading on a porous roof", *J. Wind Eng. Ind. Aerod.*, **29**(1-3), 19-28.

Chowdhury, A.G., Bitsuamlak, G., Fu, T.C. and Kawade, P. (2012), "A study on roof vents subjected to simulated hurricane effects", *Nat. Hazards*, **12**, 158-165.

DEUTSCHE NORM (2001-03), *DIN 1055-4: Einwirkungen auf Tragwerke, Teil 4: Windlasten*.

ESDU (1985), *Characteristics of Atmospheric Turbulence Near the Ground, Part II: Single Point Data for Strong Winds (Neutral Atmosphere)*, London UK.

Fernandez, G., Masters, F.J. and Gurley, K.R. (2010), "Performance of hurricane shutters under impact by roof tiles", *Eng. Struct.*, **32**(10), 3384-3393.

Florida Public Hurricane Loss Projection Model (FPHLPM) (2005), *Predicting the Vulnerability of Typical Residential Buildings to Hurricane Damage: Vol. II*, International Hurricane Research Center, Florida International University.

Gerhardt, H.J. and Janser, F. (1995), "Windbelastung belufteter Fassadensysteme", *Bauingenieur*, **70**, 193-201.

Gerhardt, H.J., Kramer, C. and Bofah, K.K. (1990), "Wind loading on loosely laid pavers and insulation boards for flat roofs", *J. Wind Eng. Ind. Aerod.*, **36**, 309-318.

Geurts, C.P.W. (2000), "Wind loads on permeable roof covering products", *Fourth Colloquium on Bluff Body Aerodynamics and Applications*, Ruhr Universität Bochum, September.

Habte, F., Asghari Mooneghi, M., Gan Chowdhury, A. and Irwin, P. (2015), "Full-scale testing to evaluate the performance of standing seam metal roofs under simulated wind loading", *Eng. Struct*., **105**, 231-248.

Harris, R.I. and Deaves, D.M. (1981), *The Structure of Strong Winds*, London, UK.

Ho, T.C.E., Surry, D., Morrish, D. and Kopp, G.A. (2005), "The UWO contribution to the NIST aerodynamic database for wind loads on low buildings: Part 1. Archiving format and basic aerodynamic data", *J. Wind Eng. Ind. Aerod*., **93**(1), 1-30.

Holmes, J.D. (2015), *Wind Loading of Structures*, 3rd Ed., CRC Press, Boca Raton, Florida.
Huang, P., Mirmiran, A., Chowdhury, A.G., Abishdid, C. and Wang, T.L. (2009), "Performance of Roof Tiles under Simulated Hurricane Impact", *J. Architect. Eng*., **15**(1), 26-34.
International Standard (2009), *ISO 4354*, Wind actions on structures.
Irwin, P. (2009), "Wind engineering research needs, building codes and project specific studies", *Proceedings of the 11th Americas Conference on Wind Engineering*, San Juan, Puerto Rico, June.
Irwin, P., Cooper, K. and Girard, R. (1979), "Correction of distortion effects caused by tubing systems in measurements of fluctuating pressures", *J. Wind Eng. Ind. Aerod*., **5**(1-2), 93-107.
Irwin, P., Dragoiescu, C., Cicci, M. and Thompson, G. (2012), "Wind tunnel model studies of aerodynamic lifting of roof pavers", *Proceedings of the Advances in Hurricane Engineering Conference*, Miami, Florida, October.
Kargarmoakhar, R., Gan Chowdhury, A. and Irwin, P. (2015), "Reynolds number effects on twin box girder long span bridge aerodynamics", *Wind Struct.*, **20**(2), 327-347.
Kind, R.J. (1994), "Predicting pressure distribution underneath loose laid roof cladding systems", *J. Wind Eng. Ind. Aerod.*, **51**(3), 371-379.
Kind, R.J., Savage, M.G. and Wardlaw, R.L. (1987), *Further wind tunnel tests of loose-laid roofing systems*, National Research Council of Canada, Report LTR-LA-294.
Kind, R.J., Savage, M.G. and Wardlaw, R.L. (1988), "Prediction of wind-induced failure of loose laid roof cladding systems", *J. Wind Eng. Ind. Aerod*., **29**(1-3), 29-37.
Kind, R.J. and Wardlaw, R.L. (1979), *Model studies of the wind resistance of two loose-laid roof-insulation systems*, National Research Council Canada, Report LTR-LA-234.
Kind, R.J. and Wardlaw, R.L. (1982), "Failure mechanisms of loose laid roof insulation systems", *J. Wind Eng. Ind. Aerod.*, **9**(3), 325-341.
Kopp, G.A. and Banks, D. (2013), "Use of the wind tunnel test method for obtaining design wind loads on roof-mounted solar arrays", *J. Struct. Eng. - ASCE*, **139**, 284-287.
Kopp, G.A., Surry, D. and Mans, C. (2005), "Wind effects of parapets on low buildings: Part 1. Basic aerodynamics and local loads", *J. Wind Eng. Ind. Aerod.*, **93**(11), 817-841.
Kumar, K.S. and Stathopoulos, T. (1998), "Spectral density functions of wind pressures on various low building roof geometries", *Wind Struct.*, **1**, 203-223.
Lin, J.X. and Surry, D. (1998), "The variation of peak loads with tributary area near corners on flat low building roofs", *J. Wind Eng. Ind. Aerod*., **77-78**, 185-196.
Lin, J.X., Surry, D. and Tieleman, H.W. (1995), "The distribution of pressure near roof corners of flat roof low buildings", *J. Wind Eng. Ind. Aerod*., **56**(2-3), 235-265.
Masters, F.J., Gurley, K.R., Shah, N. and Fernandez, G. (2010), "The vulnerability of residential window glass to lightweight windborne debris", *Eng. Struct.*, **32**(4), 911-921.
Melbourne, W.H. (1980), "Turbulence effects on maximum surface pressures – a mechanism and possibility of reduction", *Wind Eng.*, **1**, 541-551.
Mooneghi, M., Irwin, P. and Chowdhury, A. (2014), "Wind uplift of concrete roof pavers", *Proceedings of the Structures Congress 2014*, April.
NBCC (1995), *User's Guide-NBC 1995*, National Research Council of Canada, Ottawa, Canada.
NEN EN 1991-1-4/NA *Eurocode: Actions on structures – General actions – Part 1.4: Wind actions*.
Oh, J.H. and Kopp, G.A. (2012), "Pressure equalization and analytical solutions for pressures between double-layer envelopes", *Proceedings of the 3rd American Association for Wind Engineering Workshop*, Hyannis, Massachusetts, USA, August.
Oh, J.H. and Kopp, G.A. (2014), "Modelling of spatially and temporally-varying cavity pressures in air-permeable, double-layer roof systems", *Build. Environ.*, **82**, 135-150.
Oh, J.H. and Kopp, G.A. (2015), "An experimental study of pressure distributions within an air-permeable, double-layer roof system in regions of separated flow", *J. Wind Eng. Ind. Aerod.*, **138**, 1-12.
Oh, J.H., Kopp, G.A. and Inculet, D.R. (2007), "The UWO contribution to the NIST aerodynamic database for wind loads on low buildings: Part 3. Internal pressures", *J. Wind Eng. Ind. Aerod*., **95**(8), 755-779.
Pierre, L.M.S., Kopp, G.A., Surry, D. and Ho, T.C.E. (2005), "The UWO contribution to the NIST

aerodynamic database for wind loads on low buildings: Part 2. Comparison of data with wind load provisions", *J. Wind Eng. Ind. Aerod*., **93**(1), 31-59.
Richards, P.J., Hoxey, R.P., Connell, B.D. and Lander, D.P. (2007), "Wind-tunnel modelling of the Silsoe Cube", *J. Wind Eng. Ind. Aerod*., **95**(9-11), 1384-1399.
Saathoff, P.J. and Melbourne, W.H. (1997), "Effects of free-stream turbulence on surface pressure fluctuation in a separation bubble", *J. Fluid Mech.*, **337**, 1-24.
Smith, T.L. (1994), *Hurricane Andrew provides insights on roof damage*, National Roofing Contractors Association, Professional Roofing, 36-44.
Stathopoulos, T. (1982), "Wind pressure on low buildings with parapets", *J. Struct. Division*, **108**(12), 2723-2736.
Stathopoulos, T. and Baskaran, A. (1988), "Turbulent wind loading on roofs with parapet configurations", *Can. J. Civil Eng*., **29**, 570-578.
Sun, Y. and Bienkiewicz, B. (1993), "Numerical simulation of pressure distributions underneath roofing paver systems", *J. Wind Eng. Ind. Aerod*., **46-47**, 517-526.
Tieleman, H.W. (2003), "Wind tunnel simulation of wind loading on low-rise structures: a review", *J. Wind Eng. Ind. Aerod*., **91**(12-15), 1627-1649.
Trung, V., Tamura, Y. and Yoshida, A. (2010). "Numerical computation for lower surface pressures on a porous sunshade roof cover sheet", *Proceedings of the 5th International Symposium on Computational Wind Engineering (CWE2010)*, Chapel Hill, North Carolina, USA, January.
Yamada, H. and Katsuchi, H. (2008). "Wind-tunnel study on effects of small-scale turbulence on flow patterns around rectangular cylinder", *Proceedings of the 6th International Colloquium on Bluff Bodies Aerodynamics & Applications*, Italy, July.

*AD*

## Appendix: Method for obtaining 3-second gust speed from wind blow-off tests

In large-sale testing there are challenges in simulating the full wind turbulence spectrum of the natural wind mainly due to the limited size of the wind tunnels. As a result, just the high frequency part of the turbulence spectrum can be simulated adequately and low frequencies are missing as shown in Fig. 4 in the paper. A test procedure and analysis technique called Partial Turbulence Simulation (PTS) methodology was developed by Asghari Mooneghi (2014) and Asghari Mooneghi *et al*. (2015) in order to produce aerodynamic data for low-rise buildings by using large-scale models in wind tunnels and open-jet wind testing facilities like the Wall of Wind at FIU. Asghari Mooneghi (2014) showed that Eq. (A1) can be used for approximately calculating a cut-off frequency between the high frequency and the low-frequency turbulence.

$$n_c = 0.0716 \frac{U}{{}^{x}L_u} \left( \frac{I_u}{I_{uH}} \right)^3 \tag{A1}$$

where the ${}^{x}L_u$ and $U$ are the full spectrum values of longitudinal integral scale and the mean velocity respectively. $I_{uH}$ is the turbulence intensity in a partial turbulence simulation and $I_u$ is the full-spectrum longitudinal turbulence intensity. For the current problem representative values of $U = 30$ m/s, ${}^{x}L_u = 12$ m, $I_u = 0.3$ and $I_{uH} = 0.07$ were used, implying $n_c = 14$ Hz.

The cut-off frequency as calculated from the above Eq. (A1) can be used to estimate the equivalent gust-duration at full scale using (Asghari Mooneghi 2014)

$$t_{gust} = 0.45/n_c \tag{A2}$$

The derivation of the above equations is a separate topic by itself and has been described in detail in Asghari Mooneghi (2014) and Asghari Mooneghi *et al.* (2015). Using the above methodology, the equivalent gust duration at full scale for the current test is equal to 0.032 s. A moving average was performed to calculate the peak 0.03 s gust from wind speed measurements during the wind lift-off tests. In order to convert the wind lift-off speeds to a 3-second gust speed a conversion factor equal to $U_{3sec}/U_{0.03\,sec} = 0.83$ was calculated for suburban terrain at z=3.048 m (building height at full scale). The procedure for converting the wind speeds averaging time was based on Harris and Deaves (1981) model taken from ESDU (1985).